PHYSICAL REVIEW B **96**, 134119 (2017)

Switching the chirality of a ferroelectric vortex in designed nanostructures by a homogeneous electric field

Le Van Lich,[1,2,*] Takahiro Shimada,[1] Jie Wang,[3] Van-Hai Dinh,[2] Tinh Quoc Bui,[4] and Takayuki Kitamura[1]

[1]*Department of Mechanical Engineering and Science, Kyoto University, Nishikyo-ku, Kyoto 615-8540, Japan*

[2]*Department of Mechanics of Materials and Metal Forming, Hanoi University of Science and Technology, No 1, Dai Co Viet Street, Hanoi, Vietnam*

[3]*Department of Engineering Mechanics, School of Aeronautics and Astronautics, Zhejiang University, Hangzhou 310027, China*

[4]*Department of Civil and Environmental Engineering, Tokyo Institute of Technology, 2-12-1-W8-22, Ookayama, Meguro-ku, Tokyo 152-8552, Japan*

(Received 24 July 2017; revised manuscript received 10 October 2017; published 25 October 2017)

Polarization vortices that typically form in ferroelectric nanostructures are fundamental polar topological structures characterized by a curling polarization around a stable core. The control of vortex chirality by conventional fields including homogeneous electric field is a key to the utilization of vortices in technological applications. However, an effective control of the vortex chirality by such an electric field remains elusive since the toroidal moment of ferroelectric vortex is conjugated to a curled electric field rather than the homogeneous electric field. Here we demonstrate the control of vortex chirality by homogeneous electric field in free-standing nanodots with rationally designed nanostructures. The nanodots are designed by including a notch or an antinotch in the rectangular structure of nanodots. The results show that the chirality of polarization vortex is deterministically switched by a homogeneous electric field through the control of depolarization distribution by designed structures. The evolution path under homogeneous electric field in antinotched nanodot takes place in the opposite direction in comparison with that in notched nanodot. We further demonstrate that the designed nanostructures break the symmetry of electrostatic field in the ferroelectric systems, where the depolarization field concentrates at the notch but scatters at the antinotch. Such a symmetry breaking of electrostatic field results in the opposite evolution paths in the notched and antinotched nanodots under homogeneous electric field and provides the fundamental reason that allows such control. The present study suggests a new route on the practical control of the vortex domain pattern in ferroelectric nanostructures by homogeneous electric field.

DOI: 10.1103/PhysRevB.96.134119

I. INTRODUCTION

Pivotal to the further development of ferroelectrics and multiferroics is a deep understanding of the susceptibilities (particularly to electric fields) and routes to control and manipulate ferroelectric order parameter in the materials. Such knowledge has enabled variety of advanced electronic devices to be realized, such as nonvolatile random access memories [1,2], data storages [3,4], switchable photovoltaics [5,6], tunnel junctions [7,8], field-effect transistors [9,10], and magnetoelectric-coupling devices [11,12]. Until now, these applications have typically exploited the switching of polar states since the rectilinear polarization domains can be easily switched between two opposite directions by an external homogeneous electric field. On the other hand, the trend of ever-shrinking electronic circuitry brings about a decrease of ferroelectric dimensions approached to nanoscale with the aid of micro- and nanoscale manufacturing technologies. Recent theoretical studies [13,14] have shown that the screening of a depolarization field [15] in confined ferroelectrics with a size of several nanometers is enhanced through the alignment of polarization along the free surfaces, which results in the formation of closed-flux polarization ordering, i.e., polarization vortex. The polarization vortex is characterized by an in-plane curling of polarization around a stable central core, which is regarded as topological defect [16,17]. More recently, experimental studies have made great steps towards the realization of the theoretical predictions and successfully observed the polarization vortices in ferroelectric nanostructures [18–20]. These observations of polarization vortices open exciting opportunities for novel ferroelectric-based nanodevices. For instance, the bistability of vortex chirality, i.e., clockwise (CW) and counterclockwise (CCW) chiralities, is appealing for novel nonvolatile memory storage concepts [14]. Moreover, the properties of electronic transport at the polarization vortex core is quite promising for the design and implementation of integrated oxide electronic devices based on domain patterning [21]. To a reliable implementation of vortices for such applications, the prerequisite is control of the vortex chirality [22], i.e., polarization vortex switching.

However, the switching of ferroelectric vortex is a non-trivial task since the toroidal moment of a ferroelectric vortex is conjugated to a curled electric field rather than a homogeneous electric field [23]. It is thus a natural idea to utilize curled electric fields to switch ferroelectric vortices, which has been theoretically investigated on the basic of an effective Hamiltonian method [24] and phase-field simulations [25–28]. The polarization vortex has been demonstrated to be deterministically switched by the curled electric field, which is required to be large and highly localized [24–26]. On the other hand, a nonvanishing curled electric field can only be generated by a temporal change of magnetic field, according to the Maxwell's equation, $\nabla \times E = -\partial B/\partial t$. However, the magnitude of the applied magnetic field that is necessary for the switching of electric toroidal moment is somewhat

*le.lichvan.6z@kyoto-u.ac.jp; lich.levan@hust.edu.vn

impractical. Hence, many theoretical works have made efforts towards an alternative switching strategy that avoids the use of curled electric fields. For instance, transverse inhomogeneous electric fields, which are produced by charged tips near the ferroelectric nanodot, is used to switch the direction of the electric toroidal moment in ferroelectric nanodots [29]. Such control, nevertheless, requires complex implement structures and seemingly a combination of a cooling down process. Another strategy is the use of asymmetric ferroelectric rings to switch the closure-flux state by homogenous electrostatic field [30]. However, such nanorings exclude physical polarization core in the closure-flux state, which is topologically distinguished from polarization vortex [16,17]. Recently, the feasibility of vortex switching by homogenous electric field in ferroelectric nanosystems is investigated by taking into account the effects of asymmetric mechanical fields, e.g., caused by substrate, dislocations, and local clamping force [27,31,32]. Although it is possible to realize single-vortex switching by a homogeneous electric, such nanosystems further require a delicate control of crystallographic and/or mechanical fields. Therefore, an efficient control of polarization vortex by the conventionally controlled field, e.g., homogeneous electric field, remains elusive.

Pursuing an efficient control of polarization switching, we have previously demonstrated that polarization pattern and its switching behavior can be tailored by deliberately designed geometry of ferroelectric nanostructures [33] and proposed the concept of ferroelectric nanometamaterials, i.e., tuning the polarization configuration and ferroelectric properties by deliberately engineered structures rather than chemical constituents [17,33–36]. Particularly, confined geometry of ferroelectrics imposes extrinsic frustration to the polarization field through the enhancement of depolarization fields at free surfaces of the nanostructures. This geometrical frustration may even give rise to a chiral symmetry breaking in rationally designed structures such as nanosprings [37], where the chiral interactions between polarization field and external fields are induced by confined geometry of nanoscale ferroelectrics. Therefore, the use of rationally designed nanostructures is quite promising for the effective control of vortex chirality under homogeneous electric field.

In the present study, we demonstrate the control of vortex chirality by homogeneous electric field in designed nanodots, using a phase field model based on the Ginzburg-Landau theory. The phase field model is constructed incorporating to the finite element algorithm to simulate the ferroelectric system with arbitrary boundary condition and geometrical shapes. The designed nanodots are intentionally included in a notch or an antinotch. The domain evolutions of designed nanodots under homogeneous electric field are investigated and compared to that of a rectangular nanodot for clarity. In addition, the underlying origins of the vortex switching and the significant contribution of the designed nanostructures to the control of vortex chirality are investigated and discussed.

II. COMPUTATIONAL DETAILS

A. Phase field model of $PbTiO_3$ based on the Ginzburg-Landau theory

To investigate the formation of spontaneous polarization patterns in the designed nanodots and the polarization switching under homogeneous electrical field, a real-space phase field model is constructed based on the Ginzburg-Landau theory [38]. In the phase field model, the local polarization vector, $P = (P_1, P_2, P_3)$ is taken as the order parameter to describe free energies of the ferroelectric systems. The total free energy of the ferroelectric system F is obtained by integrating the total free energy density f over the entire volume of the ferroelectric system V. The total free energy density includes the Landau energy density, the gradient energy density, the elastic energy density, the coupling energy density, and the electrostatic energy density due to the external electric field, which has the expression [39–42]:

$$\begin{aligned} f = \; & f_{\text{Land}}(P_i) + f_{\text{Grad}}(P_{i,j}) \\ & + f_{\text{Elas}}(\varepsilon_{ij}) + f_{\text{Coup}}(P_i, \varepsilon_{ij}) \\ & + f_{\text{Elec}}(P_i, E_i), (i,j = 1,2,3), \end{aligned} \tag{1}$$

where $P_{i,j} = \partial P_i / x_j$ is the derivative of the ith component of the polarization vector P_i, with respect to the jth coordinate x_j; ε_{ij} and E_i denote the components of strain and electric field, respectively.

The Landau energy density is commonly expressed in terms of polarization components as [43–45]:

$$\begin{aligned} f_{\text{Land}}(P_i) = \; & \alpha_1 \sum_i (P_i)^2 + \alpha_{11} \sum_i (P_i)^4 \\ & + \alpha_{12} \sum_{i>j} (P_i)^2 (P_j)^2 + \alpha_{111} \sum_i (P_i)^6 \\ & + \alpha_{112} \sum_{i>j} [(P_i)^4 (P_j)^2 + (P_i)^2 (P_j)^4] \\ & + \alpha_{123} \prod_i (P_i)^2, \end{aligned} \tag{2}$$

where α_1 is the dielectric stiffness, and α_{11}, α_{12}, α_{111}, α_{112}, and α_{123} are higher order dielectric stiffness constants. All the higher order dielectric stiffness constants are assumed to be independent of temperature, while the dielectric stiffness constant linearly depends on the temperature according to the Curie-Weiss law, $\alpha_1 = (T - T_0)/2\kappa_0 C_0$, where T and T_0 denote the temperature and the Curie-Weiss temperature, respectively, C_0 denotes the Curie constant, and κ_0 is the dielectric constant of a vacuum [46]. The gradient energy density for ferroelectric materials represents the domain wall energy density that gives the energy penalty for the spatially inhomogeneous polarization. The gradient energy density is described by [47]:

$$f_{\text{Grad}}(P_{i,j}) = G_{ijkl} P_{i,j} P_{k,l}, \quad (k,l = 1,2,3), \tag{3}$$

where G_{ijkl} are the gradient energy coefficients. The elastic energy density induced by mechanical strain is given by:

$$f_{\text{Elas}}(\varepsilon_{ij}) = \tfrac{1}{2} c_{ijkl} \varepsilon_{ij} \varepsilon_{kl}, \tag{4}$$

where c_{ijkl} are the elastic constants. The coupling energy density between spontaneous polarization and strain is expressed by [43–45]:

$$f_{\text{Coup}}(P_i, \varepsilon_{ij}) = -q_{ijkl} \varepsilon_{ij} P_k P_l, \tag{5}$$

where q_{ijkl} are electrostrictive constants. The electrostatic energy density, which is obtained through Legendre

transformation, is expressed as [39,48]:

$$f_{\text{Elec}}(P_i, E_i) = -\tfrac{1}{2}\kappa_c E_i^2 - E_i P_i, \tag{6}$$

where κ_c is the dielectric constant of the background material.

The temporal evolution of the polarization field towards its thermodynamic equilibrium state is described by the time-dependent Ginzburg-Landau (TDGL) equation:

$$\frac{\partial P_i(r,t)}{\partial t} = -L\frac{\delta F}{\delta P_i(r,t)}, \tag{7}$$

where L is a kinetic coefficient, $\delta F/\delta P_i(r,t)$ denotes the thermodynamic driving force for the spatial and temporal evolution of the ferroelectric system, $r = (x_1, x_2, x_3)$ and t denote the spatial vector and time, respectively. In addition to Eq. (7), the following mechanical equilibrium equation and the Maxwells (or Gauss) equation must be satisfied simultaneously with respect to body force-free and charge-free ferroelectric materials:

$$\frac{\partial}{\partial x_i}\left(\frac{\partial f}{\partial \varepsilon_{ij}}\right) = 0, \tag{8}$$

and

$$\frac{\partial}{\partial x_i}\left(-\frac{\partial f}{\partial E_i}\right) = 0. \tag{9}$$

To solve the equilibrium equations, numerical algorithm based on the finite element method (FEM) is employed in the present study. Using the variation or principle of virtual work, the weak form of the governing equations (7), (8), and (9) is expressed as:

$$\begin{aligned}\int_V \Bigg[&\frac{\partial f}{\partial \varepsilon_{ij}}\delta\varepsilon_{ij} + \frac{\partial f}{\partial E_i}\delta E_i + \frac{1}{L}\frac{\partial P_i}{\partial t}\delta P_i \\ &+ \frac{\partial f}{\partial P_{i,j}}\delta P_{i,j} + \frac{\partial f}{\partial P_i}\delta P_i\Bigg] dV \\ &= \int_A \left[t_i \delta u_i - \omega\delta\phi + \left(\frac{\partial f}{\partial P_{i,j}} n_j\right)\delta P_i\right] dA,\end{aligned} \tag{10}$$

where t_i is the surface traction, u_i is displacement, ω is the surface charge, ϕ is electrical potential, $(\partial f/\partial P_{i,j})n_j$ is the surface gradient flux, and n_j is the component of the normal unit vector of the surface. For the space discretization, hexahedral elements with seven degrees of freedom at each node are employed. The seven degrees of freedom consist of three polarization components, one electrical potential variable, and three displacement components. In comparison with previous phase field simulations of ferroelectrics that use the Fourier spectral iterative perturbation algorithm [41,49], the present phase field model does not require uniform hexahedral (3D) and quadrilateral (2D) meshes and periodic boundary conditions for numerical implementation [50]. All the governing equations are solved in real space. The present phase field model is able to simulate ferroelectrics with arbitrary boundary conditions and geometrical shapes. Therefore, the real-space phase field model with FEM-based algorithm is suitable and effective for the study of domain evolution in ferroelectric nanostructures.

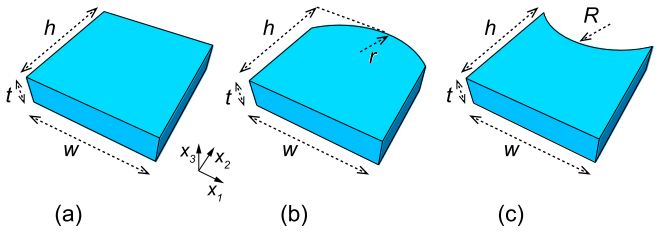

FIG. 1. Geometries of (a) rectangular nanodot, (b) antinotched nanodot, and (c) notched nanodot.

B. Simulation model and procedure

To illustrate the idea of geometrical-tailored interaction between polarization vortex and homogeneous electric field, we design nanodots with notch and antinotch. For comparison, a nanodot with rectangular shape is additionally considered. Figure 1 shows the geometries of nanodots used in the present study. To intentionally form spontaneous polarization vortex in nanodots, the dimensions of nanodots are set in a range from several to tens of nanometers, which takes into account the strong depolarization field at free surfaces of the nanodots [14,51,52]. Therefore, the thickness of nanodots t is prepared at 4 nm, while the width w and height h are set to be 16 nm. The notch and antinotch are prepared with circular curvatures, where the radii of the curves, R and r, are both taken to be 18 nm. To realize bare free surfaces of the free-standing nanodots, the mechanical boundary conditions on all free surfaces are traction free, while the electrical boundary conditions set to be open circuited, i.e., $\boldsymbol{D}\cdot\boldsymbol{n} = 0$, so that the depolarizing fields from the polar surfaces are explicitly taken into account. Noted that previous studies [34,53] have considered ferroelectric nanostructures under both general and open-circuited electrostatic boundary conditions and suggested that there is no difference in polarization domain structures under both the electrostatic boundary conditions. However, the open-circuited boundary conditions substantially simplify the calculations since it does not require the external space. Thus, in the present study, we employ the open-circuited boundary condition in consideration of computing resources. The nanodots consist of a single crystal of ferroelectric $PbTiO_3$ with the [100], [010], and [001] orientations along the x_1, x_2, and x_3 directions, respectively. The material properties used in the present study are provided in previous studies [42,51].

In order for ferroelectric nanodots to attain thermodynamic equilibrium without external fields, a random distribution of polarization with infinitesimal magnitude is introduced into the systems as an initial condition, and the evolution of the polarization field is numerically simulated by iteratively solving the TDGL equation. A backward Euler scheme and Newton iteration method are used in the FEM algorithm for the time integration and nonlinear iteration, respectively. The polarization configuration is stably formed when an insignificant change in polarization is observed. Then, an external homogeneous electric field is applied to the nanodots step-by-step along the x_1 direction with periodic triangular waves to investigate the polarization switching behavior. We use 61 points to mimic a period of the triangular wave, with E_1 gradually varying between -7×10^6 V/m and 7×10^6 V/m.

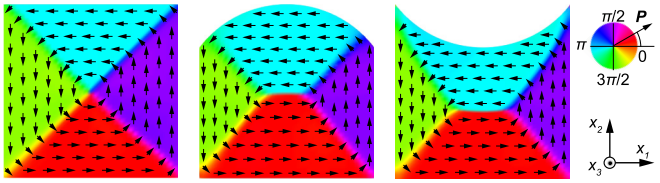

FIG. 2. Spontaneous polarization patterns in ferroelectric nanodots with (a) rectangular, (b) antinotched nanodot, and notched structures. The black arrows indicate the direction of polarization vector. The contour colors indicate the angle between the polarization vector and the x_1 direction.

At each point of E_1, the simulation time is set to be sufficiently long to ensure that the system reaches an equilibrium domain structure.

III. RESULTS AND DISCUSSION

A. Formation of polarization vortex in free-standing ferroelectric nanodots

Figure 2 shows the distribution of spontaneous polarization in the free-standing $PbTiO_3$ nanodots at the thermodynamic equilibrium state in the absence of external field. The spontaneous polarization purely orients in the x_1-x_2 plane since the polarization component in the x_3 direction is suppressed owing to a significant depolarization field induced by the strong geometrical confinement [54]. In addition, the spontaneous polarization energetically favors to align along free surfaces, while keeping the head-to-tail arrangement, and thereby, forms a circular closed-flux pattern, i.e., single polarization vortex. From our preliminary results, the single polarization vortex state is the most stable state in comparison with other states such as multiple polarization domains or multivortices. This is also consistent with that from a previous study [55], which further verifies our phase field simulation. Figure 2 shows that the polarization vortex in each nanodot has CCW chirality. Although there are two equivalent yet opposite chiralities of polarization vortex, i.e., CW and CCW, that can be formed in the nanodots, only the CCW polarization vortex is described here and is consistently adopted as initial polarization pattern for the consideration of polarization vortex switching. The characteristics of the polarization vortex obtained in the present study are consistent with those of preceding studies [14,51,52], which indicates the reliability of present phase field simulations. The polarization vortex is characterized by toroidal moment of polarization G_3, which is defined as $G_3 = \frac{1}{V}\int_V r_i \times P_i dV$, where r_i is the position vector of polarization P_i and V is volume of the nanodot. The direction of toroidal moment vector is perpendicular to the vortex plane, which is along the x_3 direction in the present study. Magnitudes of toroidal moments are determined equal 4.24, 4.22, and 3.94 e/Å for rectangular, antinotched, and notched nanodots, respectively. Since the chiralities and magnitudes of toroidal moment in all three types of nanodot are almost the same, the characteristics of spontaneous polarization vortex are insensitive to the geometry of nanodots.

B. Rectangular nanodot under a homogeneous electric field

To gain an insight into the effect of geometrical nanostructures on the polarization vortex switching, we investigate the polarization evolution of the antinotched and notched nanodots under a homogeneous electric field in comparison with that in the rectangular nanodot. The obtained results for the free-standing rectangular nanodot are firstly presented for clarity.

Figure 3 shows the domain evolution of free-standing rectangular nanodot under a triangular wave of homogeneous electric field E_1. The initial state polarization pattern is taken with the spontaneous CCW single vortex, as shown in Fig. 2(a). From our preliminary simulations, the net of polarization in the x_2 direction keeps equal zero regardless of the magnitude of applied electric field E_1 due to the formation of equivalent yet opposite direction along the x_2 axis of polarization domains. Thus, the consideration regarded to the net polarization in the x_2 direction is eliminated in the present study. Figure 3(a) shows the toroidal moment G_3 and the average polarization in the x_1 direction P_1^{ave} as functions of E_1. The average polarization is determined as $P_1^{\text{ave}} = (\sum_{j=1}^{n} P_1^j)/n$, where n is the total number of nodes in the FEM models and P_1^j is the magnitude of P_1 at the jth node. The evolution direction is marked by several typical points from A0 to A10. The corresponding polarization domain patterns from point A0 to A10 are depicted in Fig. 3(b). At the first electrical increase process from A0 to A3, as E_1 increases from 0 to 7×10^6 V/m, the average polarization P_1^{ave} monotonically increases from 0 to about 1.15 C/m^2, while the toroidal moment G_3 decreases from 4.24 e/Å to 0. An observation of the domain structures reveals that the initial single vortex (A0) evolves into a polar domain pattern where all polarization vectors align along the direction of the applied electric field (A3), which causes the drop in the magnitude of toroidal moment. In the electrical decrease process from A3 to A5, as E_1 decreases from 7×10^6 V/m to 0, the average polarization P_1^{ave} monotonically decreases, while the toroidal moment G_3 keeps a constant equal to zero. The corresponding domain structures indicate a transformation of the polar state to vortex state. This implies that the polar state is only stable at a large enough field region [56]. Although the vortex state can be achieved at low field region, the nanodot adopts a double-vortices state instead of reforming a single-vortex state. This is because of two equivalent nucleation sites at the top and bottom surfaces of the nanodot. As the field E_1 further decreases from 0 to -7×10^6 V/m, the double-vortices state evolves into a polar state with its polarization along the opposite direction to x_1, as depicted in Fig. 3(b) from A5 to A8. At the second electrical increase process from A8 to A10, as E_1 increases from -7×10^6 V/m to 0, a transformation of polar state to vortex state happens and a double-vortices state is reformed. The net toroidal moment vanishes at all points during the evolution A3 to A10, because of the formation of polar state or double vortices with opposite chiralities. Comparing state A5 with state A10, the chiralities of the double-vortices state have been switched by the homogeneous field E_1, which is similar to that previously predicted in rectangular systems [27]. Therefore, single-vortex switching in the free-standing rectangular nanodot by a homogeneous electric field is prohibited due to the formation of double-vortices state.

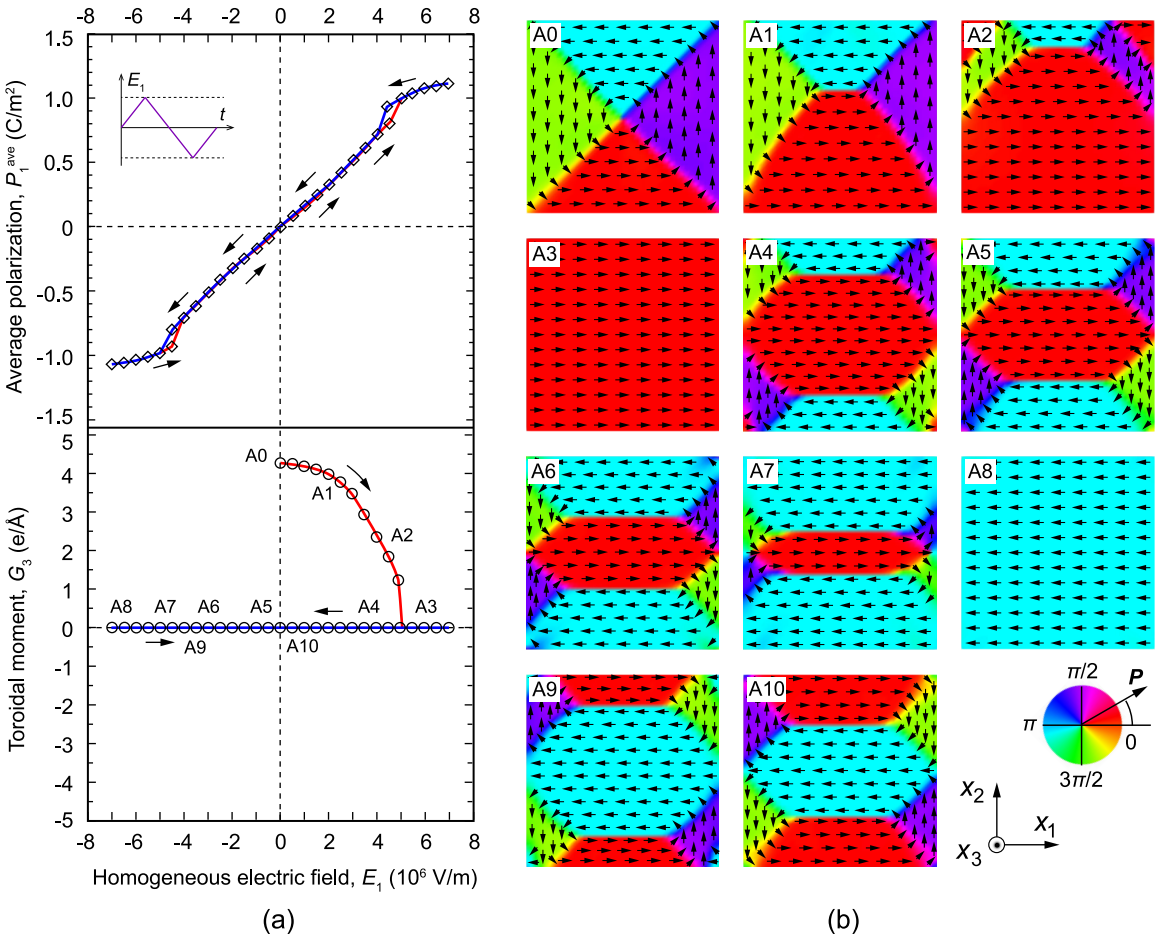

FIG. 3. Domain evolution of free-standing rectangular nanodot under a triangular wave of homogeneous electric field along the x_1 direction, E_1. (a) Average polarization P_1^{ave} and toroidal moment G_3 as functions of E_1. Direction of the evolution is indicated by black arrows and marked by several points from A0 to A10. (b) The corresponding domain structures from point A1 to A10.

C. Antinotched nanodot under a homogeneous electric field

Figure 4 shows the domain evolution of the antinotched nanodot under a triangular wave of homogeneous electric field E_1. Unlike the rectangular nanodot, clear $P_1^{ave}-E_1$ and G_3-E_1 hysteresis loops are exhibited in Fig. 4(a), indicating a switching of the polarization vortex by the homogeneous field. The initial polarization structure of antinotched nanodot adopts a CCW single-vortex state, as depicted at B0 in Fig. 4(b). At the first electrical increase process from B0 to B3, as E_1 increases from 0 to 7×10^6 V/m, the vortex state transforms into a polar state, manifested with a decrease of G_3 and an increase of P_1^{ave}. The toroidal moment drops to zero value when E_1 is as large as 5×10^6 V/m. The domain evolution and the evolution paths during the first increase process in the antinotched nanodot are almost identical to that in the rectangular nanodot shown in Fig. 3. In the electrical decrease process from B3 to B6, as E_1 decreases from 7×10^6 V/m to 0, the polar state is remained E_1 is larger than 2.5×10^6 V/m, then transforms into a single-vortex state. Because of the polar-to-vortex transformation, the magnitude of P_1^{ave} suddenly decreases, while the magnitude of G_3 abruptly increases. Importantly, the newly formed vortex (B6) has CW chirality, which is opposite to the initial CCW chirality (B0). This demonstrates a success of single-vortex switching in the antinotched nanodot. It is interesting to find that the direction of the dipoles at the antinotch region is intact as the polar-to-vortex transformation occurs. In the subsequent poling under a negative field E_1 from B6 to B9, the direction of dipoles at the antinotch is inversed, and thereby, forming a polar domain structure. However, the direction of dipoles at the antinotch is conserved in the increase process from B9 to B0, leading to the reforming of CCW polarization vortex (B0). Therefore, the polarization vortex can be deterministically switched by a homogeneous electric field via transition to intermediate polar state, in which the direction of polarization in the antinotched region determines whether the CW or CCW polarization vortices survive.

To characterize and elucidate the details of the polar-to-vortex transformation in the antinotched nanodot, temporal evolution of domain structure at the homogeneous electric field $E_1 = 2.5 \times 10^6$ V/m during the electrical decrease process is considered. Figures 5(a) and 5(b) show the toroidal moment G_3 and average polarization P_1^{ave} as functions of computational time and typical snapshots during the temporal evolution of domain structure in the antinotched nanodot, respectively. At the beginning of the evolution, G_3 has zero value of magnitude since the polar domain structure dominates the entire antinotched nanodot. Subsequently, G_3 quickly decreases in

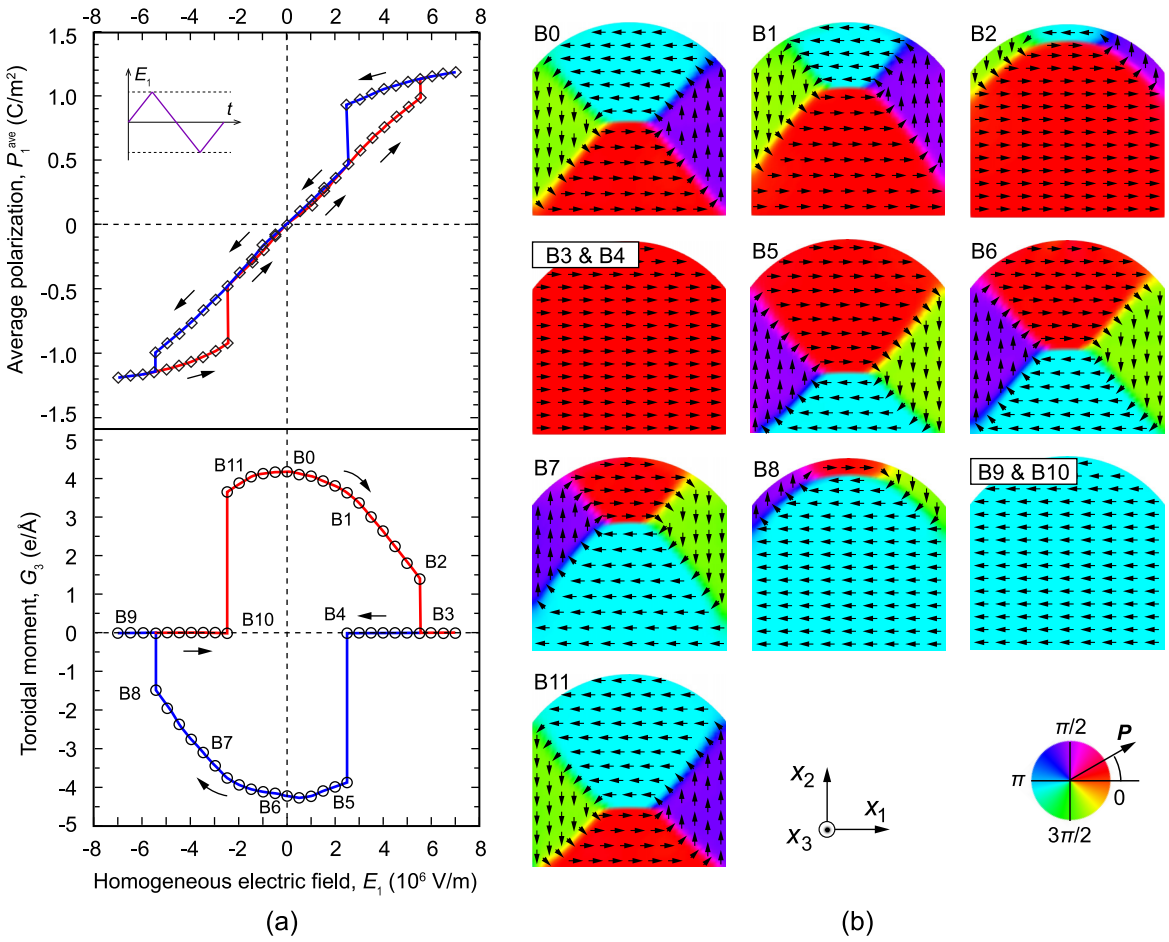

FIG. 4. Domain evolution of free-standing antinotched nanodot under a triangular wave of homogeneous electric field along the x_1 direction, E_1. (a) Average polarization P_1^{ave} and toroidal moment G_3 as functions of E_1. Direction of the evolution is indicated by black arrows and marked by some special points from B0 to B11. (b) The corresponding domain structures from point B0 to B11.

its magnitude during the evolution and then gradually reaches to constant after substantial time steps, where the equilibrium of the system achieves. The magnitude of P_1^{ave}, meanwhile, gradually decreases during the evolution, then reaches to a constant after substantial time steps. The snapshots of the polarization patterns during the temporal evolution from B′1 to B′6 in Fig. 5(b) show that the polarization firstly changes by reversing its orientation at local area near the bottom surface of the antinotched nanodot. The changing polarization area then quickly expands to the left and right sides of the antinotched nanodot during the evolution. Noted that the 90° switching occurs on the left and right sides of the antinotched nanodot to arrange the polarization along free surfaces, which help to reduce the depolarization field. On the other hand, the direction of dipoles at the antinotch region is intact during the temporal evolution. When the system reaches to the equilibrium state, the CW polarization vortex is dominant, the domain structure of the antinotched nanodot. Therefore, direction of polarization in the antinotch region is preserved in the polar-to-vortex transformation, which determines the chirality of vortex after the transformation in the antinotched nanodot.

D. Notched nanodot under a homogeneous electric field

Figure 6 shows the domain evolution of the notched nanodot under the triangular wave of homogeneous electric field E_1. The initial polarization structure of the notched nanodot also adopts CCW single-vortex state, as depicted at C0 in Fig. 6(b). According to our preliminary simulations, to achieve complete hysteresis loops of $P_1^{ave} - E_1$ and $G_3 - E_1$ after one periodic of the triangular wave, the homogeneous electric field should be started with a decrease process. Therefore, a periodic of the triangular wave starts with a decrease process of homogeneous electric field is taken for the consideration of domain evolution in the notched nanodot, as shown in Fig. 6(a). Although the $P_1^{ave} - E_1$ hysteresis loop in the notched nanodot is almost identical to that in the antinotched nanodot, the behavior of $G_3 - E_1$ hysteresis loop is inversely. At the first electrical decrease process from C0 to C3, as E_1 decreases from 0 to -7×10^6 V/m, the vortex state transforms into a polar state, where all polarization vectors arrange in the direction of applied electric field. During the process, the toroidal moment gradually decreases with the decrease of the applied electric field, then drops to zero value when E_1 is as large as -5×10^6 V/m. In the electrical increase process from

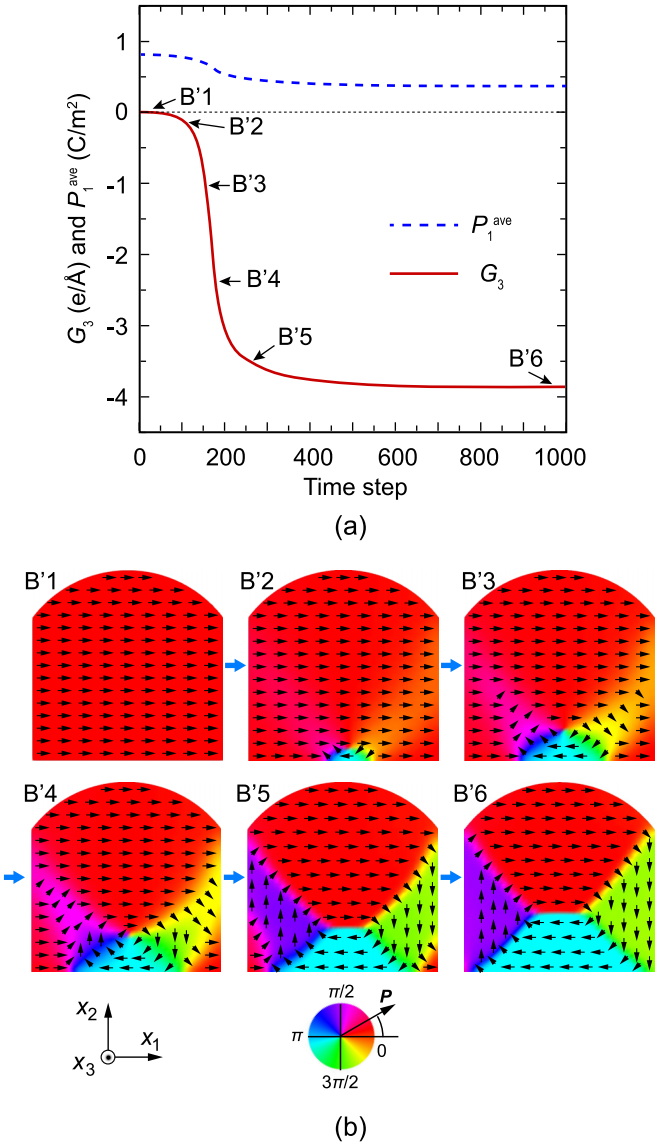

FIG. 5. Temporal evolution of domain structure during the polar-to-vortex transformation. (a) Toroidal moment G_3 and average polarization P_1^{ave} as functions of simulated time. (b) Snapshots of the polarization patterns during the polar-to-vortex transformation in the antinotched nanodot.

C3 to C6, as E_1 increases from -7×10^6 V/m to 0, the polar state remains until E_1 equals -2.5×10^6 V/m then transforms into a single-vortex state. The newly formed vortex (C6) has CW chirality, which is opposite to the initial CCW chirality (C0). This demonstrates a success of single-vortex switching in the notched nanodot. As the polar-to-vortex transformation occurs, the polarization near the tip of the notch reverses its direction, while the polarization near the bottom surface remains. In the subsequent increase process under positive field E_1 from C6 to C9, the direction of polarization near the bottom surface is inversed, which results in a polar state along the x_1 direction. However, the direction of polarization at the notch is reversed in the subsequent decrease process from C9 to C0, leading to the reforming of CCW polarization vortex (C0). Therefore, the polarization vortex can be deterministically switched by a homogeneous electric field, in which the chirality of vortex is determined by direction of polarization at the flat surface that is opposite to the notch.

To characterize the reforming of polarization vortex in the notched nanodot, temporal evolution of domain structure under the homogeneous electric field $E_1 = 2.5 \times 10^6$ V/m during the decrease process is considered in comparison with that in the antinotched nanodot. Figures 7(a) and 7(b) show the toroidal moment G_3 and average polarization P_1^{ave} as functions of computational time and typical snapshots during the temporal evolution of domain structure in the notched nanodot, respectively. At the beginning of the evolution, G_3 has zero value of magnitude since the polar domain structure dominates the entire notched nanodot. Then, the magnitude of G_3 quickly increases during the temporal evolution and gradually reaches to constant after substantial time steps, where the equilibrium of the system achieves. Inversely, the magnitude of P_1^{ave} gradually decreases during the temporal evolution, then reaches to a constant after substantial time steps. The snapshots of the polarization patterns during the temporal evolution from C′1 to C′6 in Fig. 7(b) show that the polarization firstly changes near the tip of the notch by the local 180° switching. The changing polarization area then quickly expands to the left and right sides of the notched nanodot, where the 90° switching occurs to align the polarization along the free surfaces. The arrangement of polarization along free surfaces helps to reduce the depolarization field. On the other hand, the direction of dipoles at the bottom surface of notched nanodot is intact during the evolution. When the system reaches to the equilibrium state, the CCW polarization vortex dominates the domain structure of the notched nanodot. Therefore, the change of polarization at the notch region triggers the polar-to-vortex transformation.

E. Discussion

To understand the switching of vortex in asymmetry ferroelectrics, a previous study [30] has defined a vector R characterizing the system asymmetry. The cross product of this vector with the electric field, $R \times E$, can be considered as a field able to interact with G in asymmetric ferroelectrics because both are axial vectors. Unlike previous studies, where vector R represents the asymmetry-induced shift in the center of gravity of the ring, here we define vector R as a spatial vector from the centroid of nanodot to the vortex core. The interaction energy in asymmetric ferroelectrics is directly proportional to $(R \times E) \cdot G$. Figures 4(a) and 4(b) show that the change of toroidal moment to the applied homogeneous electric field is gradually from point B0 to B1 where the vortex core is closed to the centroid of the antinotched nanodot, i.e., small R and thus small interaction energy. However, the change becomes faster from point B1 to B2 as the vortex core is far from the centroid, i.e., relatively large R and high interaction energy. Similar tendency is also observed in notched nanodot, as shown in Figs. 6(a) and 6(b). Therefore, the vortex switching in asymmetry nanodots under homogeneous electric field can be achieved owning to the susceptibility of G with the cross product of $R \times E$.

Note that the switching phenomenology in nanodots from the present study is somewhat similar to that in nanorings from

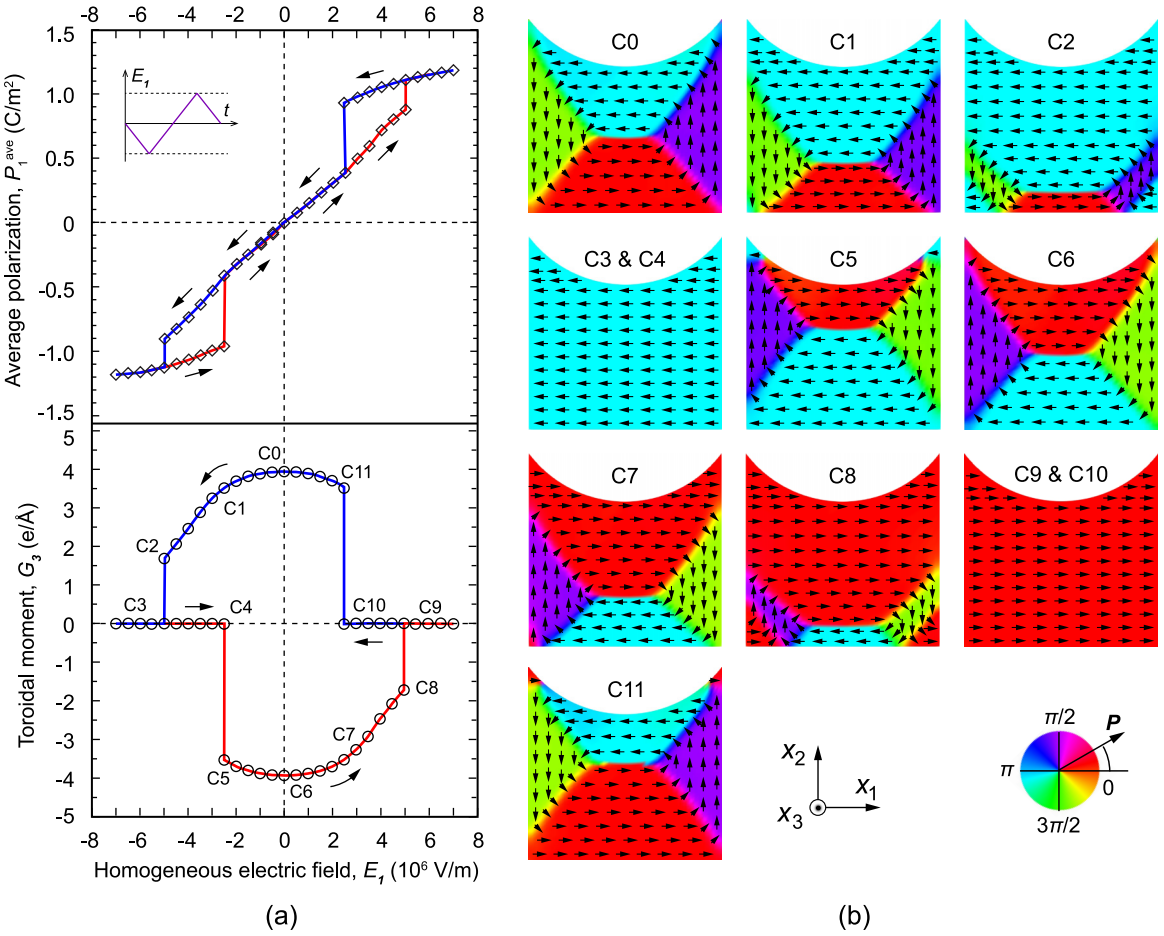

FIG. 6. Domain evolution of free-standing notched nanodot (initially with a polarization vortex structure) under a triangular wave of homogeneous electric field along the x_1 direction, E_1. (a) Average polarization P_1^{ave} and toroidal moment G_3 as functions of E_1. Direction of the evolution is indicated by black arrows and marked by some special points from C0 to C11. (b) The corresponding domain structures from point C0 to C11.

previous studies [30,57]. However, the difference between the polarization topology in nanodots with vortex core and in nanorings without the core gives rise to some important aspects that distinguish the vortex switching in nanodots from that in nanorings. Particularly, the appearance of vortex core is the main source for the interaction between the polarization vortex in nanodot and the homogeneous electric field. For example, in Figs. 4 and 6, the vortex structure in nanodots initially responds to the applied homogeneous electric field at the vortex core, subsequently, the position of the vortex core is changed depending on the magnitude of the electric field. This is because the highest energy density, i.e., instability, is located at the vortex core since the continuously spatial change of polarization near the core induces large gradient energy and large elastic strain energy through the coupling between the polarization and the strain [26]. In addition, the distance between vortex core and the centroid of nanodots also affects the switching behavior through the interaction energy, as discussed above. Therefore, the vortex core plays a significant role in the switching of polarization vortex in nanodots, where the vortex structure is gradually changed according to the magnitude of electric field through a successive shift in position of vortex core. In a sharp contrast, the vortex structure in nanoring is changed dramatically under homogeneous electric field. For instance, an antiferrotoroidic state with the formation of two opposite chirality vortices occurs as an intermediate state [30,57]. Although there is one vortex core appearing in such an antiferrotoroidic state, this core plays an insignificant role in the vortex switching of nanorings, which is distinguished from that in the proposed nanodots. On the other hand, our proposed nanodots achieve an advantage with a higher magnitude of toroidal moment in the absence of the external electric field compared to that of proposed nanorings, which is useful for the implementation of polarization vortex for memory devices.

Given the domain evolutions in the rectangular, antinotched, and notched nanodots, it is clearly seen that the vortex chirality can be deterministically switched by homogeneous electric field through the intermediate polar state if the reformation of single polarization vortex from polar state is achieved. To clarify the underlying mechanisms responsible for the deterministically reformation of single polarization vortex from polar state in antinotched and notched nanodots, the distribution of depolarization field is investigated. Figure 8 shows distributions of depolarization field at the beginning of the temporal evolution of polar-to-vortex transformations

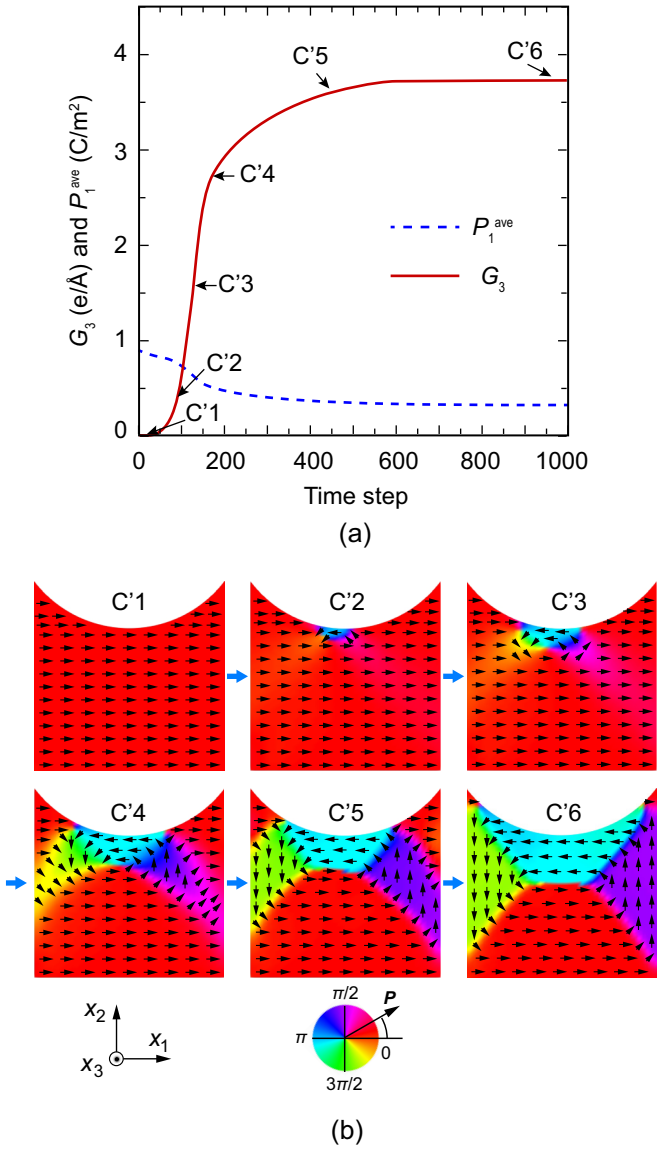

FIG. 7. Temporal evolution of domain structure during the polar-to-vortex transformation. (a) Toroidal moment G_3 and average polarization P_1^{ave} as functions of simulated time. (b) Snapshots of the polarization patterns during the formation of polarization vortex in notched nanodot.

in antinotched and notched nanodots. For comparison, the distribution of depolarization field in the rectangular nanodot is also presented. Figures 8(d)–8(f) show that the distribution of depolarization field is homogeneous in the rectangular nanodot but inhomogeneous in both antinotched and notched nanodots. Particularly, in the antinotched nanodot, the strength of depolarization field is low in the antinotch area due to the scatter of depolarization field, while it is relatively high near the bottom surface. The scatter of depolarization field at the antinotch area helps to preserve the polarization direction in this region during the polar-to-vortex transformation. Contrarily, the relatively high depolarization brings about the change of polarization occurring firstly near the bottom surface that triggers the evolution of polarization structure, as shown in Fig. 5. On the other hand, in the notched nanodot, the

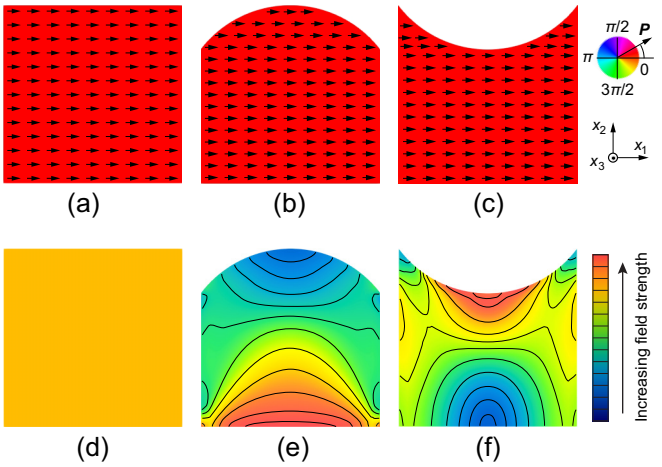

FIG. 8. Polar domain structures in (a) rectangular, (b) antinotched, and (c) notched nanodots. Distribution of depolarization field in (d) rectangular, (e) antinotched, and (f) notched nanodots corresponded to the polar state depicted in (a)–(c), respectively.

depolarization field highly concentrates near the notch area, while its strength is moderate near the bottom surface. The high concentration of depolarization results in the change of polarization near the notch at the beginning of the polar-to-vortex transformation, as shown in Fig. 7. The concentration of the field near the notch yet scatter at the antinotch is similar to that obtained in previous study [58,59]. Therefore, the inhomogeneous distribution of depolarization field results in the deterministically switching of polarization vortex shown in Figs. 4 and 6. Such depolarization field can be tailored by geometry of nanodots, where the antinotch helps to scatter the depolarization field while the notch concentrates the field.

IV. CONCLUSION AND OUTLOOK

In summary, taking into account the effects of confined geometry in ferroelectric nanostructures, we have investigated the complicated evolution of polarization vortex in designed nanodots with notch and antinotch structures under homogeneous electric field, using the real-space phase field model based on the Landau-Ginzburg theory. The characteristics of the domain evolution in different nanodot systems have been revealed and compared comprehensively. The results show that designed nanodots exhibit distinct evolution paths from the rectangular ones in response to homogeneous electric field. The present study demonstrates that single vortex can be deterministically switched by a homogeneous electric field through controlling the shape of nanodots. The designed nanostructures break the symmetry of electrostatic field in the ferroelectric systems, where the depolarization field concentrates at the notch but scatters at the antinotch. Such a symmetry breaking of electrostatic field results in the opposite evolution paths in the notched and antinotched nanodots under homogeneous electric field.

The dependence of vortex switching behavior on the shape of a ferroelectric nanostructure may hold the key to the miniaturization of ferroelectric-based memories. In the vortex-based memory elements, any geometric, morphological, or physical

variations of notch and/or antinotch and along the edges of the elements can cause significant changes in the switching field threshold. The design of geometry to achieve a much smaller switching electric field is thus quite promising. The rich and fascinating phenomena exhibited by designed nanostructures depend intricately on the shape and size. The engineering of patterned ferroelectric nanostructures with well-defined memory state and robust, repeatable, and uniform polarization switching characteristics is a fertile area for exploring future ferroelectric and multiferroics devices. On the other hand, ferroelectric nanostructures are usually fabricated on substrates, which gives rise to the substrate-induced strain. Since strain can interact with both polarization and toroidal moment [36] through the electromechanical coupling, the substrate-induced strain alters somehow the polarization vortex switching under homogeneous electric field. For instance, the appearance of substrate-induced strain can enhance or reduce the magnitude of the switching electric field. Thus, the present study poses a fundamental yet important question on the effect of substrate-induced strain on the polarization vortex switching under homogeneous electric field. Ultimately, since the nanodot can be considered as an internal constituent of ferroelectric integrated structures, the present study opens exciting opportunities for tailoring ferroelectric and related properties through rational engineering of internal nanostructures on the basic of the ferroelectric nanometamaterials concept. This, on the other hand, would further drive metamaterials researches. Therefore, the present study would stimulate efforts from both experimentation and simulation works to explore more efficient routes to control the chirality of polarization vortex and achieve novel or even unprecedented functionalities in ferroelectric nanometamaterials.

ACKNOWLEDGMENT

This work was supported in part by JSPS KAKENHI Grants No. 25000012, No. 17H03145, and No. 17K18824.

[1] J. F. Scott, *Ferroelectric Memories*, 2nd ed. (Springer Verlag, Berlin, 2000).
[2] R. E. Jones, P. D. Maniar, R. Moazzami, P. Zurcher, J. Z. Witowski, Y. T. Lii, P. Chu, and S. J. Gillespie, Thin Solid Films **270**, 584 (1995).
[3] T. Tybell, C. H. Ahn, and J. M. Triscone, Appl. Phys. Lett. **72**, 1454 (1998).
[4] Y. Cho, K. Fujimoto, Y. Hiranaga, Y. Wagatsuma, A. Onoe, K. Terabe, and K. Kitamura, Appl. Phys. Lett. **81**, 4401 (2002).
[5] T. Choi, S. Lee, Y. J. Choi, V. Kiryukhin, and S. Cheong, Science **324**, 63 (2009).
[6] Z. Xiao, Y. Yuan, Y. Shao, Q. Wang, Q. Dong, C. Bi, P. Sharma, A. Gruverman, and J. Huang, Nat. Mater. **14**, 193 (2015).
[7] E. Y. Tsymbal and H. Kohlstedt, Science **313**, 181 (2006).
[8] V. Garcia, S. Fusil, K. Bouzehouane, S. Enouz-Vedrenne, N. D. Mathur, A. Barthelemy, and M. Bibes, Nature (London) **460**, 81 (2009).
[9] S. L. Miller and P. J. McWhorter, J. Appl. Phys. **72**, 5999 (1992).
[10] S. Mathews, R. Ramesh, T. Venkatesan, and J. Benedetto, Science **276**, 238 (1997).
[11] T. Zhao, A. Scholl, F. Zavaliche, K. Lee, M. Barry, A. Doran, M. P. Cruz, Y. H. Chu, C. Ederer, N. A. Spaldin, R. R. Das, D. M. Kim, S. H. Baek, C. B. Eom, and R. Ramesh, Nat. Mater. **5**, 823 (2006).
[12] H. W. Jang, D. Ortiz, S.-H. Baek, C. M. Folkman, R. R. Das, P. Shafer, Y. Chen, C. T. Nelson, X. Pan, R. Ramesh, and C.-B. Eom, Adv. Mater. **21**, 817 (2009).
[13] H. Fu and L. Bellaiche, Phys. Rev. Lett. **91**, 257601 (2003).
[14] I. I. Naumov, L. Bellaiche, and H. Fu, Nature (London) **432**, 737 (2004).
[15] R. R. Mehta, B. D. Silverman, and J. T. Jacobs, J. Appl. Phys. **44**, 3379 (1973).
[16] N. D. Mermin, Rev. Mod. Phys. **51**, 591 (1979).
[17] L. Van Lich, T. Shimada, J. Wang, and T. Kitamura, Nanoscale **9**, 15525 (2017).
[18] Y. L. Tang, Y. L. Zhu, X. L. Ma, A. Y. Borisevich, A. N. Morozovska, E. A. Eliseev, W. Y. Wang, Y. J. Wang, Y. B. Xu, Z. D. Zhang, and S. J. Pennycook, Science **348**, 547 (2015).
[19] A. K. Yadav, C. T. Nelson, S. L. Hsu, Z. Hong, J. D. Clarkson, C. M. Schlepütz, A. R. Damodaran, P. Shafer, E. Arenholz, L. R. Dedon, D. Chen, A. Vishwanath, A. M. Minor, L. Q. Chen, J. F. Scott *et al.*, Nature (London) **530**, 198 (2016).
[20] C. M. Dudhe, S. J. Khambadkar, and N. V. Dhoke, Scr. Mater. **131**, 89 (2017).
[21] N. Balke, B. Winchester, W. Ren, Y. H. Chu, A. N. Morozovska, E. A. Eliseev, M. Huijben, R. K. Vasudevan, P. Maksymovych, J. Britson, S. Jesse, I. Kornev, R. Ramesh, L. Bellaiche, L. Q. Chen *et al.*, Nat. Phys. **8**, 81 (2012).
[22] J. Hlinka, J. Privratska, P. Ondrejkovic, and V. Janovec, Phys. Rev. Lett. **116**, 177602 (2016).
[23] V. M. Dubovik and V. V. Tugushev, Phys. Rep. **187**, 145 (1990).
[24] I. I. Naumov and H. Fu, Phys. Rev. Lett. **101**, 197601 (2008).
[25] J. Wang and M. Kamlah, Phys. Rev. B **80**, 012101 (2009).
[26] J. Wang, Appl. Phys. Lett. **97**, 192901 (2010).
[27] W. J. Chen and Y. Zheng, Acta Mater. **88**, 41 (2015).
[28] L. Van Lich, T. Shimada, J. Wang, and T. Kitamura, Acta Mater. **112**, 1 (2016).
[29] S. Prosandeev, I. Ponomareva, I. Kornev, I. Naumov, and L. Bellaiche, Phys. Rev. Lett. **96**, 237601 (2006).
[30] S. Prosandeev, I. Ponomareva, I. Kornev, and L. Bellaiche, Phys. Rev. Lett. **100**, 047201 (2008).
[31] W. J. Chen, Y. Zheng, B. Wang, and J. Y. Liu, J. Appl. Phys. **115**, 214106 (2014).
[32] F. Xue, L. Li, J. Britson, Z. Hong, C. A. Heikes, C. Adamo, D. G. Schlom, X. Pan, and L.-Q. Chen, Phys. Rev. B **94**, 100103 (2016).
[33] L. Van Lich, T. Shimada, S. Sepideh, J. Wang, and T. Kitamura, Acta Mater. **125**, 202 (2017).
[34] T. Shimada, L. Van Lich, K. Nagano, J. Wang, and T. Kitamura, Sci. Rep. **5**, 14653 (2015).
[35] L. Van Lich, T. Shimada, K. Miyata, K. Nagano, J. Wang, and T. Kitamura, Appl. Phys. Lett. **107**, 232904 (2015).
[36] L. Van Lich, T. Shimada, S. Sepideh, J. Wang, and T. Kitamura, Acta Mater. **113**, 81 (2016).
[37] T. Shimada, L. Van Lich, K. Nagano, J.-S. Wang, J. Wang, and T. Kitamura, Sci. Rep. **6**, 35199 (2016).

[38] J. Slutsker, A. Artemev, and A. Roytburd, Phys. Rev. Lett. **100**, 087602 (2008).
[39] H.-L. Hu and L.-Q. Chen, J. Am. Ceram. Soc. **81**, 492 (1998).
[40] L.-Q. Chen, Annu. Rev. Mater. Res. **32**, 113 (2002).
[41] Y. L. Li, S. Y. Hu, Z. K. Liu, and L. Q. Chen, Appl. Phys. Lett. **78**, 3878 (2001).
[42] J. Wang, S.-Q. Shi, L.-Q. Chen, Y. Li, and T.-Y. Zhang, Acta Mater. **52**, 749 (2004).
[43] A. F. Devonshire, Philos. Mag. **40**, 1040 (1949).
[44] A. F. Devonshire, Philos. Mag. **42**, 1065 (1951).
[45] A. F. Devonshire, Adv. Phys. **3**, 85 (1954).
[46] M. J. Haun, E. Furman, S. Jang, H. McKinstry, and L. Cross, J. Appl. Phys. **62**, 3331 (1987).
[47] W. Cao and L. E. Cross, Phys. Rev. B **44**, 5 (1991).
[48] J. Wang, Y. Li, L.-Q. Chen, and T.-Y. Zhang, Acta Mater. **53**, 2495 (2005).
[49] Y. L. Li, S. Y. Hu, Z. K. Liu, and L. Q. Chen, Acta Mater. **50**, 395 (2002).
[50] P. Song, T. Yang, Y. Ji, Z. Wang, Z. Yang, L. Chen, and L. Chen, Commun. Comput. Phys. **21**, 1325 (2017).
[51] L. Van Lich, T. Shimada, K. Nagano, Y. Hongjun, J. Wang, K. Huang, and T. Kitamura, Acta Mater. **88**, 147 (2015).
[52] A. R. Balakrishna and J. E. Huber, Appl. Phys. Lett. **106**, 092906 (2015).
[53] J. Wang and M. Kamlah, Eng. Fract. Mech. **77**, 3658 (2010).
[54] N. Ng, R. Ahluwalia, and D. J. Srolovitz, Acta Mater. **60**, 3632 (2012).
[55] L. Lahoche, I. Luk'Yanchuk, and G. Pascoli, Integr. Ferroelectr. **99**, 60 (2008).
[56] I. Naumov and H. Fu, Phys. Rev. Lett. **98**, 077603 (2007).
[57] S. Prosandeev, I. Ponomareva, I. Naumov, I. Kornev, and L. Bellaiche, J. Phys.: Condens. Matter **20**, 193201 (2008).
[58] M. McMillen, R. G. P. McQuaid, S. C. Haire, C. D. McLaughlin, L.-W. Chang, A. Schilling, and J. M. Gregg, Appl. Phys. Lett. **96**, 042904 (2010).
[59] J. R. Whyte, R. G. P. McQuaid, P. Sharma, C. Canalias, J. F. Scott, A. Gruverman, and J. M. Gregg, Adv. Mater. **26**, 293 (2014).